

Monitoring multiple distances within a single molecule using switchable FRET

Stephan Uphoff¹, Seamus J Holden¹, Ludovic Le Reste¹, Javier Periz¹, Sebastian van de Linde², Mike Heilemann² & Achillefs N Kapanidis¹

The analysis of structure and dynamics of biomolecules is important for understanding their function. Toward this aim, we introduce a method called 'switchable FRET', which combines single-molecule fluorescence resonance energy transfer (FRET) with reversible photoswitching of fluorophores. Typically, single-molecule FRET is measured within a single donor-acceptor pair and reports on only one distance. Although multipair FRET approaches that monitor multiple distances have been developed, they are technically challenging and difficult to extend, mainly because of their reliance on spectrally distinct acceptors. In contrast, switchable FRET sequentially probes FRET between a single donor and spectrally identical photoswitchable acceptors, dramatically reducing the experimental and analytical complexity and enabling direct monitoring of multiple distances. Our experiments on DNA molecules, a protein-DNA complex and dynamic Holliday junctions demonstrate the potential of switchable FRET for studying dynamic, multicomponent biomolecules.

Single-molecule methods have changed the landscape of biological physics and biochemistry by focusing on the fundamental unit of molecular analysis: an individual molecule^{1,2}. A popular single-molecule method is fluorescence resonance energy transfer (FRET) spectroscopy²⁻⁴, which relies on a distance-dependent dipole-dipole interaction between a donor and an acceptor fluorophore to report biomolecular structure, dynamics and interactions⁵. The versatility of FRET has recently been extended by alternating-laser excitation (ALEX) schemes that monitor the relative donor-acceptor stoichiometry⁶.

Although single-molecule FRET usually involves a single donor-acceptor pair, one can also use multiple pairs to probe multiple intramolecular distances, enabling distance triangulation or multi-angulation⁷ and multiperspective monitoring of conformational changes. Because of molecular heterogeneity and dynamics, obtaining multidistance information from a single molecule is preferable to combining information from populations of single molecules, each carrying a single FRET pair at different positions and measured in separate experiments. To this end, multicolor methods using three or more distinct fluorophores

have been developed, including three-color FRET^{8,9} and three-color ALEX¹⁰ techniques. Such experiments are complicated: they require site-specific labeling with fluorophores exhibiting large spectral overlap for FRET yet having sufficient spectral separation to allow detection in three or more separate emission regions. Moreover, FRET between multiple fluorophores follows a cascade of energy-transfer processes, complicating data analysis and interpretation⁹. As a result, multicolor FRET methods cannot be easily extended, and as such, they have not realized their potential.

Here we describe switchable FRET, a method that can be used to probe two or more distances in a single molecule by using a single donor and two or more identical acceptors. Using only two types of fluorophores circumvents many problems of the multicolor approaches and allows the examination of multiple FRET pairs in a single molecule. Specifically, switchable FRET uses temporal confinement of fluorescence (that is, sorting fluorescence by time in addition to sorting by absorption or emission characteristics) to sequentially probe multiple FRET pairs. Temporal confinement is achieved by photoswitching^{11,12} (that is, reversible modulation of fluorophore absorption), a process exploited in super-resolution imaging^{13,14} and in ensemble FRET modalities^{15,16}. As photoswitching can be induced in many fluorophores^{17,18} our method is general and extendable. Moreover, probing of several switching states per molecule allows calculation of accurate FRET efficiencies, aiding efforts to deduce structural information from single molecules^{7,19,20}. The number of distances measured by switchable FRET is fundamentally limited only by our FRET resolution.

Using switchable FRET, we measured two accurate FRET efficiencies and corresponding distances in a single DNA molecule. To demonstrate the general applicability of switchable FRET, we probed two distances within a protein-DNA complex. Finally, we used switchable FRET to directly monitor conformational changes in single dynamic Holliday junctions from two perspectives.

RESULTS

Concept

Switchable FRET is compatible with various types of fluorophores such as carbocyanine Cy5 and oxazine ATTO655 that undergo switching via different mechanisms^{11,12,18} (Fig. 1a,b).

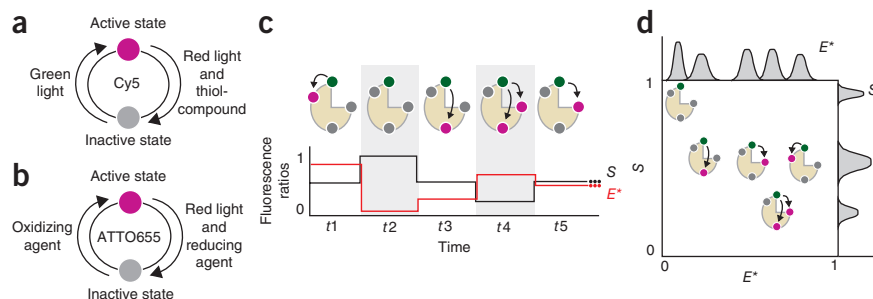
¹Biological Physics Research Group, Department of Physics, University of Oxford, Oxford, UK. ²Applied Laser Physics & Laser Spectroscopy, Bielefeld University, Bielefeld, Germany. Correspondence should be addressed to A.N.K. (a.kapanidis1@physics.ox.ac.uk).

Figure 1 | Concept of switchable FRET.

(a) Irradiation of Cy5 with red light reads out the fluorescence signal and switches the fluorophore from the active fluorescent state to the inactive dark state; this transition requires thiol-containing reducing agents and oxygen removal. Irradiation with green light supports the transition back to the active state.

(b) ATTO655 reversibly switches in presence of a reducing agent and molecular oxygen upon irradiation at a single wavelength: the inactive dark state is reached by intersystem crossing and reduction from the active fluorescent state. Spontaneous oxidation restores the fluorescent state.

(c) To probe multiple distances via FRET, a single molecule is labeled with one donor (green) and multiple identical photoswitchable acceptors (magenta). ALEX of individual immobilized molecules provides information on apparent FRET (E^*) and stoichiometry (S). Single-pair FRET states (t_1 , t_3 and t_5) are probed by switching the acceptors between an active state and an inactive state (gray) that does not interact with the donor. Transient donor-only states (t_2) or states with more than one active acceptor (t_4) can be identified by a change in stoichiometry. (d) The E^* and S data are summarized on a two-dimensional scatter plot with projected one-dimensional histograms at the sides. Different states appear as distinct clusters in the histogram and can be sorted using E^* and S .



In switchable FRET, immobilized molecules labeled with a single donor and multiple identical acceptors are probed over time by reversibly switching acceptors between a dark state with an absorption spectrum that does not overlap with the donor emission spectrum (and does not participate in FRET) and a fluorescent state that participates normally in FRET (Fig. 1c). Stochastic switching separates the time segments of individual active acceptors, thus resolving multiple FRET pairs at different positions on a single molecule in a temporal fashion. The apparent FRET efficiency, E^* , reports the distance between the donor and the active acceptor. Reversible switching between active and inactive states interrogates each pair many times, a feature that permits monitoring structural changes in a molecule.

We used ALEX to probe FRET and the stoichiometry ratio (S) of active donor and acceptor fluorophores simultaneously^{6,21}. Because the donor was not switchable in our experiments, S served as a ‘counter’ of the number of active acceptors at any time: donor-only states had high S values (Fig. 1c); states with a donor and a single active acceptor had intermediate S values, and states with one donor and two active acceptors display low S values. We summarized the FRET and stoichiometry information of an individual molecule on a two-dimensional E^* - S histogram (Fig. 1d).

Proof of principle

As a proof-of-principle experiment for switchable FRET, we prepared a 55 base pair (bp) DNA with a single Cy3B donor placed between two Cy5 acceptors (Supplementary Table 1). The distal and proximal donor-acceptor separations were 19 bp and 10 bp, respectively. One molecule could adopt four distinct photophysical states; namely (i) donor-only (denoted as 0-D0, in which ‘D’ stands for donor, ‘0’ stands for an acceptor in its inactive state, and ‘-’ denotes the 19-bp separation; 10-bp separation is implied between D and the second 0) when both acceptors were inactive, (ii) state A-D0 (low E^* , intermediate S) when only the distal acceptor (A) was active; (iii) state 0-DA (high E^* , intermediate S) when only the proximal acceptor was active; and (iv) state A-DA (high E^* , low S) when both acceptors were active.

We measured immobilized DNA molecules using total internal reflection fluorescence (TIRF) microscopy combined with ALEX²¹. A typical time trace of fluorescence intensity, E^* and S (an ‘ALEX time trace’; Fig. 2a) from a single DNA molecule

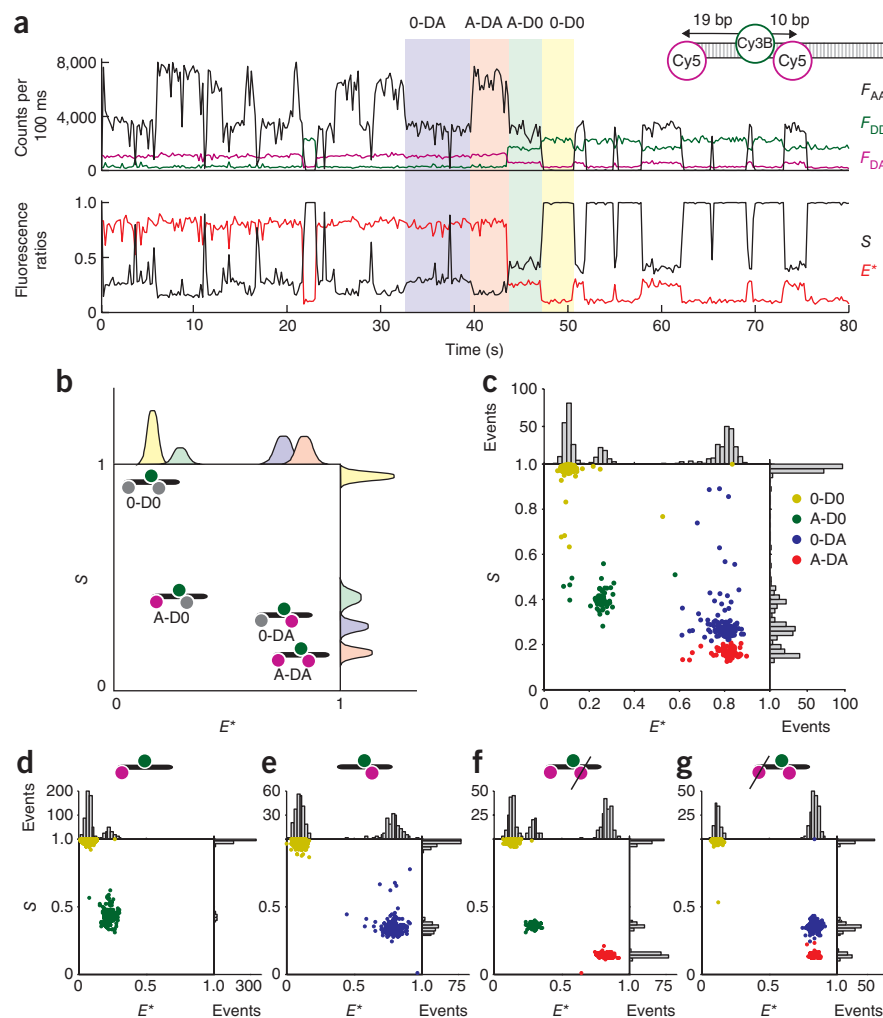
with one Cy3B and two Cy5 fluorophores showed that alternating red and green excitation caused stochastic photoswitching of the two acceptors, apparent from steps between three intensity levels in the acceptor emission upon acceptor excitation (F_{AA}). The intensity was maximal when both acceptors were active (~8,000 photon counts per 100 ms; state A-DA), intermediate during segments when only one acceptor is active (~4,000 photon counts per 100 ms; either state A-D0 or 0-DA) and low during donor-only segments (<100 photon counts per 100 ms; state 0-D0). Donor excitation yields donor emission (F_{DD}) and acceptor emission owing to FRET (F_{DA}). Because the donor transfers energy only to active acceptors, F_{DD} is maximal for 0-D0 but becomes substantially quenched when an acceptor switches on; each of the four states is adopted several times. The donor was not affected by the switching conditions and did not blink or bleach during the experiment (data not shown). We also observed that the photoactivation rate of Cy5 depended on the proximity to an activator fluorophore¹¹ and thus differed for the two acceptors in our system as indicated by their individual off-state dwell times in the ALEX time traces (data not shown).

The E^* - S histogram from the time trace in Figure 2a shows the expected four clusters representing the states 0-D0, A-D0, 0-DA and A-DA (Fig. 2b,c). To identify states and extract statistical information, we separated the clusters using a standard clustering algorithm (k means). The identified distributions were narrow ($\sigma(E^*) = \sim 0.03$), compared to typical diffusion-based FRET histograms¹⁹. The two clusters of the single-pair FRET efficiencies (E^* was 0.256 for A-D0 and 0.793 for 0-DA) were clearly separated from states 0-D0 and A-DA, and identified as individual states.

Controls

To exclude the possibility that the single-pair FRET efficiency is altered by light absorption of the second acceptor in the inactive state, we studied the same DNA with a single acceptor either at 10-bp or 19-bp separation from the donor (Supplementary Table 1). The controls showed clusters identical to those from the two-acceptor DNA (Fig. 2d,e). To test the requirement for switching to probe multiple distances, we analyzed DNA with one donor and two acceptors under nonswitching conditions²²; in this case, irreversible sequential acceptor bleaching reported on only one of the two pairs per molecule. If the proximal acceptor bleached first, the 0-DA state was missing from the E^* - S histogram (Fig. 2f);

Figure 2 | Proof-of-principle of switchable FRET. **(a)** ALEX time trace for an individual immobilized DNA molecule labeled with a single Cy3B donor separated from two Cy5 acceptors by 10-bp (high FRET) and 19-bp (low FRET). ALEX of the donor and the acceptor yields photon streams F_{DD} , F_{DA} and F_{AA} , which are used for calculating E^* and S . The colored backgrounds highlight a switching sequence of all four states. **(b)** Expected locations of the four clusters on the E^* - S histogram: 0-D0 at high S and low E^* , A-D0 at intermediate S and low E^* , 0-DA at intermediate S and high E^* , and A-DA at low S and high E^* . **(c)** The E^* - S histogram of the data from **a** shows the four expected clusters, identified with a clustering algorithm. **(d,e)** Controls using DNA labeled with one donor and either the distal **(d)** or proximal acceptor **(e)** (experimental conditions are as in **a**). **(f,g)** Cy5-Cy3B-Cy5 controls under nonswitching conditions. For the molecule in **f**, the proximal acceptor bleaches first, whereas in **g**, the distal acceptor bleaches first.



when the distal acceptor bleached first, the A-D0 state was missing (**Fig. 2g**).

To confirm that the information from a single molecule reflects a substantial fraction of all molecules, we combined the E^* - S histograms of 147 molecules (**Supplementary Fig. 1b**). Approximately 57% of fully labeled molecules adopted all four states (for statistics for all samples see **Supplementary Table 2**); this number is now limited by irreversible photobleaching and the stochastic nature of photoswitching. The mean E^* and S values differed slightly between molecules because of intermolecule heterogeneity and optical aberrations, which broaden the distributions in the combined histogram. The match between the combined and single-molecule data demonstrated robustness of switchable FRET.

Accurate FRET from a single molecule

Switchable FRET also permitted calculation of accurate FRET efficiencies (E) for a single molecule (**Supplementary Fig. 2**), a feature important for experiments that generate constraints for structural analysis of biomolecular complexes^{19,20,23}. Recovering accurate FRET requires corrections for cross-talk between signals and detection biases (by measuring the detection-correction factor γ (ref. 19)). Switchable FRET provided all the data for the corrections from an individual molecule (**Supplementary Table 3**): (i) the donor-only state 0-D0 (for donor-leakage correction); (ii) an acceptor-only state A-00 or 0-0A (for acceptor direct excitation correction; obtained from the same molecule if the donor bleaches before both acceptors bleach⁸, or by using a switchable donor), and (iii) the A-D0 and 0-DA states (for γ correction). The ability to calculate accurate FRET from an individual molecule is useful when correction factors differ between molecules (for example, owing to changes in the local fluorophore environment).

We compared experimentally determined FRET efficiencies of the states to theoretical values of the FRET efficiency assuming a cylindrical model of B-DNA¹⁹ (**Supplementary Table 3**). Direct conversion of accurate FRET efficiencies to distances required accurate assumption of rotational freedom of fluorophores, validated by anisotropy experiments (Online Methods). The structural parameters that yielded theoretical FRET efficiencies consistent with our experimental data were in good agreement with other DNA models based on FRET^{19,24}, providing support for the use of switchable FRET as a quantitative tool.

Switchable FRET with an alternative acceptor

To show the generality of switchable FRET, we tested ATTO655, a FRET acceptor that switches without the need of a second wavelength for its reactivation^{17,18} (**Fig. 1b**); instead, reactivation occurs through oxidation. We used the same labeling configuration as for Cy5-Cy3B-Cy5 (**Supplementary Table 1**). An example ALEX time trace shows the fluctuations in the F_{AA} signal owing to stochastic acceptor photoswitching (**Fig. 3a**). Under our experimental conditions, ATTO655 switched more rapidly than Cy5, capturing both FRET states in a shorter time (**Fig. 3b**). The ability to control rapid switching by irradiation intensity, as well as reducer and oxidizer concentration, should enable switchable FRET to study fast molecular dynamics.

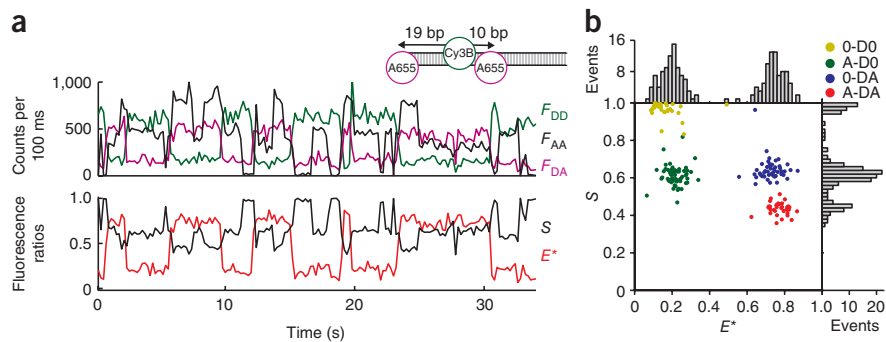


Figure 3 | Switchable FRET with an alternative acceptor. **(a)** ALEX time trace for an individual immobilized DNA molecule labeled with a single Cy3B donor separated from two ATTO655 (A655) acceptors by 10 bp (high E^*) and 19 bp (low E^*). **(b)** The E^* - S histogram shows the four expected clusters: 0-D0 at high S and low E^* , A-D0 at intermediate S and low E^* , 0-DA at intermediate S and high E^* , and A-DA at lower S and high E^* .

Monte Carlo simulation

To explore the limits of switchable FRET, we performed Monte Carlo simulations for molecules containing a single donor and an arbitrary number of acceptors. We created a simulated ALEX time trace for a molecule with one donor and four acceptors (with $E = 0.2, 0.4, 0.6$ and 0.8 ; **Supplementary Fig. 3a**). The resulting E^* - S histogram showed the expected four single-pair FRET clusters at the S segment from 0.3 to 0.6 (D:A = 1:1; **Supplementary Fig. 3b**). These results can be interpreted more easily than data representing four distances probed with multicolor FRET using four different emission channels. In fact, the number of distances accessible to switchable FRET is fundamentally limited only by FRET resolution, that is, the width of single FRET distributions. For illustration purposes, the E^* - S histogram of a simulated 800 s time trace shows also rare states with multiple active acceptors (**Supplementary Fig. 3c**).

Comparisons of experimental and simulated data for the Cy5-Cy3B-Cy5 DNA (**Supplementary Fig. 4a,b**) indicated that our simple model (**Supplementary Fig. 5**) accurately described our experimental system. Widths of experimental and simulated FRET distributions were in good agreement, demonstrating that noise in our experiments can be explained by modeled photon shot noise, background noise and camera amplification noise (**Supplementary Fig. 4c**); the experimental stoichiometry

distribution was twofold larger than our model predicted (**Supplementary Fig. 4d**) mostly owing to additional blinking of Cy5 and fluctuations in laser intensities. We have also analyzed in detail the various sources of noise and factors limiting FRET resolution²⁵. The close resemblance of experimental and simulated data suggests that, with proper control of photoswitching and photobleaching, switchable FRET should be able to monitor four or more distances in a single molecule.

Protein-DNA complex

To explore the potential of switchable FRET to probe structure and interactions of proteins and their complexes, we studied the complex of DNA with catabolite

activator protein (CAP, also known as cyclic AMP receptor protein (CRP)). CAP is a global transcriptional activator that controls > 100 genes in bacteria by binding upstream of gene promoters in the presence of cAMP²⁶. Crystallographic analysis²⁷ and ensemble FRET experiments²⁸ showed that CAP bends DNA by 80°–90° upon binding.

In our experimental design, we used the homodimeric structure of CAP (**Fig. 4a**) to introduce two copies of switchable acceptor Alexa Fluor 647 (ref. 14), a hydrophilic carbocyanine fluorophore similar to Cy5. We incorporated a Cy3B donor on the 5' end of the top strand of a 39-bp dsDNA fragment containing the twofold-symmetric CAP recognition sequence (**Supplementary Table 1**). TIRF imaging of immobilized CAP-DNA complexes resulted in colocalized donor and acceptor emission spots, and enabled switchable FRET measurements (**Fig. 4b**). The E^* - S histogram showed a high and a low FRET state at intermediate stoichiometry, representing energy transfer to the acceptor on the proximal and distal subunit, respectively (**Fig. 4c**). The single-molecule data agreed well with a combined dataset of 33 molecules measured under identical conditions (**Supplementary Fig. 6**).

Probing conformational dynamics from multiple perspectives

To explore the ability to use switchable FRET to monitor conformational dynamics, we directly observed conformational changes

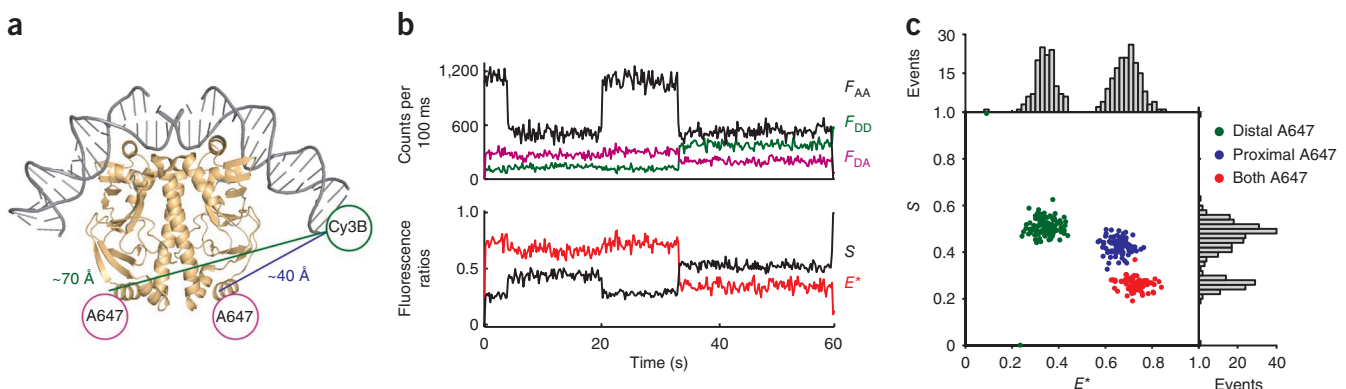
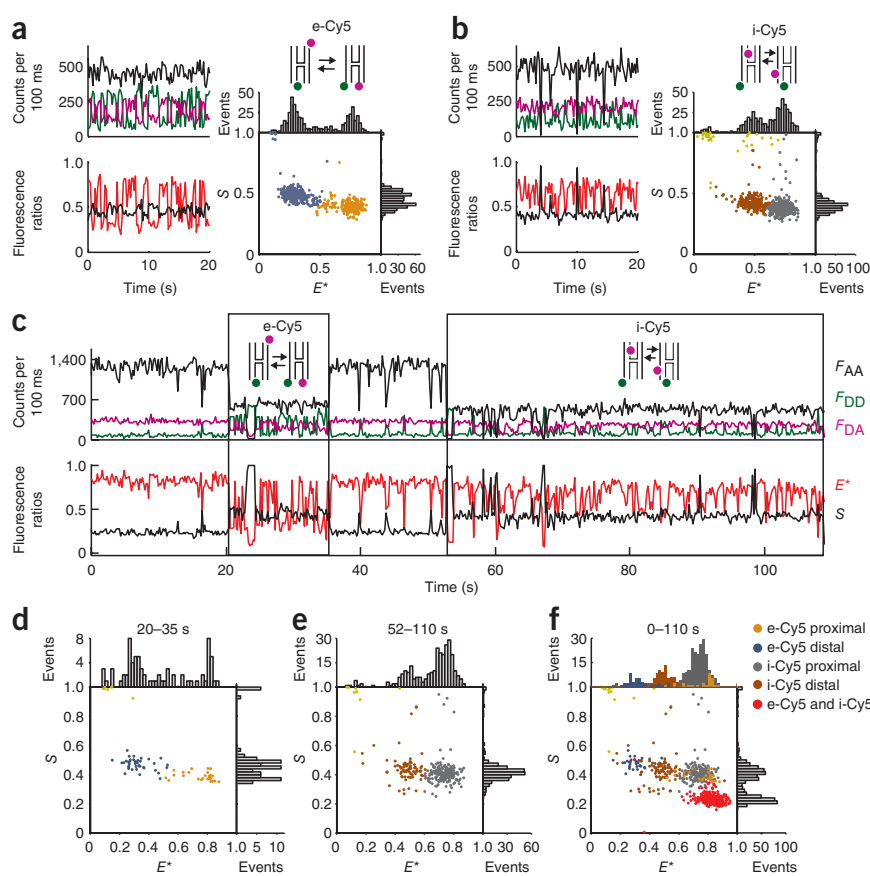


Figure 4 | Switchable FRET monitors two distances within the CAP-DNA complex. **(a)** Crystal structure of the CAP-DNA complex²⁷. CAP is in yellow, DNA is in gray, Alexa Fluor 647 (A647) and Cy3B fluorophores indicated schematically. Distances are measured between the DNA axis and the $C\alpha$ of Cys17. **(b)** ALEX time trace. **(c)** E^* - S histogram that corresponds to the time trace in **b**.

Figure 5 | Holliday junction dynamics probed from two perspectives. (a) Only Cy3B and e-Cy5 present. (b) Only Cy3B and i-Cy5 present. (c) Switchable FRET measures structural changes within a single Holliday junction from two perspectives: e-Cy5 is active in the first box, i-Cy5 is active in the second box. (d) E^* - S histograms of the first boxed region in c. (e) E^* - S histograms of the second boxed region in c. (f) E^* - S histogram of the full time trace. Cluster analysis was performed on separate time sections of the dataset to recover the states in d and e. Only single-pair FRET states are shown in the E^* histogram for clarity.

in individual DNA Holliday junctions from two perspectives, facilitating comparisons to a multicolor FRET study of a similar system⁸. In the presence of magnesium ions, the Holliday junction adopts two alternative stacked X-like structures^{8,29}, the interconversion of which is central to DNA repair and genetic recombination. We designed four DNA strands that hybridize such that a Cy3B donor at the end of one branch exhibits FRET to an end-labeled Cy5 (e-Cy5) and an internally labeled Cy5 (i-Cy5), each on a different branch (Fig. 5 and Supplementary Table 1). Owing to incomplete labeling, some molecules had only a single FRET pair. For the pair of Cy3B and e-Cy5, fluctuations between a low and a high FRET state showed conformational changes in one part of the Holliday junction (Fig. 5a; $E^* = \sim 0.3$ and $E^* = \sim 0.8$). Molecules with only Cy3B and i-Cy5 also showed FRET fluctuations but between two intermediate FRET states, consistent with the smaller distance range of the internal acceptor (Fig. 5b; $E^* = \sim 0.5$ and $E^* = \sim 0.7$); because frame rates and dynamic rates were similar for this construct, we also observed a distribution of FRET values between the two states. In agreement with previous findings, we observed a small conformer bias, with the e-Cy5 pair preferring the low FRET state and the i-Cy5 pair preferring the high FRET state⁸.

We used switchable FRET to probe conformational changes of a single molecule from two perspectives provided by two switchable acceptors (Fig. 5c). When both e-Cy5 and i-Cy5 were active (0–21 s relative to the beginning of movie acquisition), FRET was constant and high, showing that at least one acceptor was close to the donor in either conformation. Then i-Cy5 switched off, allowing e-Cy5 to monitor dynamics of the Holliday junction from one perspective (21–35 s). After a time segment with both acceptors active, only i-Cy5 remained active and probed conformational changes from a different perspective (55–110 s). E^* - S histograms displayed clusters in agreement with the single-acceptor data (Fig. 5d,e). Although the high-FRET states of e-Cy5 and i-Cy5 overlapped, temporal confinement by clear photoswitching events could easily identify four distinct single-pair FRET states in one molecule (Fig. 5f). Approximately 8% of fully labeled molecules adopted all four FRET states (Supplementary Table 2). Control experiments with a strictly doubly labeled sample



(Cy3B and e-Cy5), as well as combined single-molecule data support our results (Supplementary Fig. 7).

Additional Monte Carlo simulations confirmed that assignment of transient FRET states to multiple photoswitching acceptors was not limited to the regime in which photoswitching was slow compared to the structural dynamics (Supplementary Fig. 8). If photoswitching and dynamics occur on the same timescale, transitions in FRET resulting from structural changes can be distinguished from photoswitching events because the latter always involve an obligatory intermediate donor-only state or states with multiple active acceptors. Ultimately, in the regime in which photoswitching is faster than the dynamic rates, each transient structure can be examined from multiple perspectives, providing unique insight into multidimensional trajectories of conformational changes.

DISCUSSION

Compared to multicolor FRET approaches, switchable FRET simplifies labeling, data acquisition and data analysis. Additional development should identify optimal fluorophores and conditions for their use, allowing extension to more acceptors; such developments should also increase the yield of molecules adopting all single-pair FRET states. Given our current FRET resolution²⁵, we anticipate that extensions to more than two pairs will be straightforward.

Our results demonstrate that switchable FRET can be used to probe multiple distances in single protein molecules and protein-DNA complexes and pave the way for work on other multimeric proteins (for example, dimeric and multimeric transcription

factors, helicases and membrane proteins), which are difficult to label site-specifically with single fluorophores but are easy to label with multiple identical fluorophores. Notably, many proteins have only few surface-exposed reactive cysteine residues and thus are immediately amenable for use in switchable FRET experiments without mutagenesis. Switchable FRET will enable studies of their structure and dynamics in solution, complementing available crystallographic information. In the absence of prior information about expected distances, FRET states can still be assigned to the corresponding acceptor based on control experiments with single acceptors, and the fully labeled sample uncovers heterogeneity and dynamic interplay between states. Increased temporal resolution and higher excitation intensities for faster switching can be achieved using confocal microscopy, which can reach photoswitching timescales several-fold faster than standard TIRF microscopy (S.U. and A.N.K.; unpublished data). Hidden Markov modeling is ideally suited to recover the rates of dynamics and link transient FRET states to active acceptors³⁰. Finally, small and fast conformational dynamics below the current temporal and spatial resolution (such as the DNA dynamics that may exist within the CAP-DNA complex²⁸) can be probed based on the variance of FRET distributions³¹. These features, together with the ability to extract accurate FRET efficiencies, make switchable FRET a promising tool for probing structure and dynamics at the single-molecule level.

METHODS

Methods and any associated references are available in the online version of the paper at <http://www.nature.com/naturemethods/>.

Note: Supplementary information is available on the Nature Methods website.

ACKNOWLEDGMENTS

We thank K. Gryte, J. Hohlbein, T.M.C. Rito and A. Riegert for technical and editorial assistance, and M. Leake for suggestions. S.U., S.J.H., L.L.R., J.P. and A.N.K. were supported by a UK Bionanotechnology Interdisciplinary Research Collaboration grant, Engineering and Physical Science Research Council grant EP/D058775 and European Community Seventh Framework Programme (FP7/2007-2013) grant HEALTH-F4-2008-201418 (entitled READNA). S.U. was supported by the German National Academic Foundation and the company SAP AG. M.H. and S.v.d.L. were supported by the Systems Biology Initiative (Forschungseinheiten der Systembiologie) of the German Ministry of Research and Education (0315262).

AUTHOR CONTRIBUTIONS

S.U., M.H. and A.N.K. designed research; S.U. performed experiments and simulations; S.U. and S.J.H. analyzed data; L.L.R. built experimental setup; S.U., J.P. and S.v.d.L. prepared reagents; S.U. and A.N.K. wrote manuscript; and S.U., S.J.H., L.L.R., J.P., S.v.d.L., M.H. and A.N.K. discussed results and commented on the manuscript.

COMPETING FINANCIAL INTERESTS

The authors declare no competing financial interests.

Published online at <http://www.nature.com/naturemethods/>.

Reprints and permissions information is available online at <http://npg.nature.com/reprintsandpermissions/>.

- Selvin, P. & Ha, T. (eds). *Single Molecule Techniques: A Laboratory Manual* 1st edn. (Cold Spring Harbor Laboratory Press, Cold Spring Harbor, New York, 2008).
- Kapanidis, A.N. & Strick, T. Biology, one molecule at a time. *Trends Biochem. Sci.* **34**, 234–243 (2009).
- Roy, R., Hohng, S. & Ha, T. A practical guide to single-molecule FRET. *Nat. Methods* **5**, 507–516 (2008).
- Gadella, T. (ed.). *FRET and FLIM Techniques* 1st edn. (Elsevier, London, 2009).
- Clegg, R.M. Fluorescence resonance energy transfer and nucleic acids. *Methods Enzymol.* **211**, 353–388 (1992).
- Kapanidis, A.N. *et al.* Fluorescence-aided molecule sorting: Analysis of structure and interactions by alternating-laser excitation of single molecules. *Proc. Natl. Acad. Sci. USA* **101**, 8936–8941 (2004).
- Muschielok, A. *et al.* A nano-positioning system for macromolecular structural analysis. *Nat. Methods* **5**, 965–971 (2008).
- Hohng, S., Joo, C. & Ha, T. Single-molecule three-color FRET. *Biophys. J.* **87**, 1328–1337 (2004).
- Clamme, J.-P. & Deniz, A.A. Three-color single-molecule fluorescence resonance energy transfer. *ChemPhysChem* **6**, 74–77 (2005).
- Lee, N.K. *et al.* Three-color alternating-laser excitation of single molecules: monitoring multiple interactions and distances. *Biophys. J.* **92**, 303–312 (2007).
- Bates, M., Blosser, T.R. & Zhuang, X. Short-range spectroscopic ruler based on a single-molecule optical switch. *Phys. Rev. Lett.* **94**, 108101 (2005).
- Heilemann, M., Margeat, E., Kasper, R., Sauer, M. & Tinnefeld, P. Carbocyanine dyes as efficient reversible single-molecule optical switch. *J. Am. Chem. Soc.* **127**, 3801–3806 (2005).
- Rust, M.J., Bates, M. & Zhuang, X. Sub-diffraction-limit imaging by stochastic optical reconstruction microscopy (STORM). *Nat. Methods* **3**, 793–795 (2006).
- Heilemann, M. *et al.* Subdiffraction-resolution fluorescence imaging with conventional fluorescent probes. *Angew. Chem. Int. Edn Engl.* **47**, 6172–6176 (2008).
- Mao, S. *et al.* Optical lock-in detection of FRET using synthetic and genetically encoded optical switches. *Biophys. J.* **94**, 4515–4524 (2008).
- Jares-Erijman, E.A. & Jovin, T.M. FRET imaging. *Nat. Biotechnol.* **21**, 1387–1395 (2003).
- Vogelsang, J., Cordes, T., Forthmann, C., Steinhauer, C. & Tinnefeld, P. Controlling the fluorescence of ordinary oxazine dyes for single-molecule switching and superresolution microscopy. *Proc. Natl. Acad. Sci. USA* **106**, 8107–8112 (2009).
- Heilemann, M., van de Linde, S., Mukherjee, A. & Sauer, M. Super-resolution imaging with small organic fluorophores. *Angew. Chem. Int. Edn Engl.* **48**, 6903–6908 (2009).
- Lee, N.K. *et al.* Accurate FRET measurements within single diffusing biomolecules using alternating-laser excitation. *Biophys. J.* **88**, 2939–2953 (2005).
- Wozniak, A.K., Schröder, G.F., Grubmüller, H., Seidel, C.A. & Oesterhelt, F. Single-molecule FRET measures bends and kinks in DNA. *Proc. Natl. Acad. Sci. USA* **105**, 18337–18342 (2008).
- Margeat, E. *et al.* Direct observation of abortive initiation and promoter escape within single immobilized transcription complexes. *Biophys. J.* **90**, 1419–1431 (2006).
- Rasnik, I., McKinney, S.A. & Ha, T. Nonblinking and long-lasting single-molecule fluorescence imaging. *Nat. Methods* **3**, 891–893 (2006).
- Mekler, V. *et al.* Structural organization of bacterial RNA polymerase holoenzyme and the RNA polymerase-promoter open complex. *Cell* **108**, 599–614 (2002).
- Clegg, R.M., Murchie, A.I., Zechel, A. & Lilley, D.M. Observing the helical geometry of double-stranded DNA in solution by fluorescence resonance energy transfer. *Proc. Natl. Acad. Sci. USA* **90**, 2994–2998 (1993).
- Holden, S.J. *et al.* Defining the limits of single-molecule FRET resolution in TIRF microscopy. *Biophys. J.* (in the press).
- Lawson, C.L. *et al.* Catabolite activator protein: DNA binding and transcription activation. *Curr. Opin. Struct. Biol.* **14**, 10–20 (2004).
- Napoli, A.A., Lawson, C.L., Ebricht, R.H. & Berman, H.M. Indirect readout of DNA sequence at the primary-kink site in the CAP-DNA complex: recognition of pyrimidine-purine and purine-purine steps. *J. Mol. Biol.* **357**, 173–183 (2006).
- Kapanidis, A.N., Ebricht, Y.W., Ludescher, R.D., Chan, S. & Ebricht, R.H. Mean DNA bend angle and distribution of DNA bend angles in the CAP-DNA complex in solution. *J. Mol. Biol.* **312**, 453–468 (2001).
- Karymov, M., Daniel, D., Sankey, O.F. & Lyubchenko, Y.L. Holliday junction dynamics and branch migration: Single-molecule analysis. *Proc. Natl. Acad. Sci. USA* **102**, 8186–8191 (2005).
- McKinney, S.A., Joo, C. & Ha, T. Analysis of single-molecule FRET trajectories using hidden Markov modeling. *Biophys. J.* **91**, 1941–1951 (2006).
- Santoso, Y. *et al.* Conformational transitions in DNA polymerase I revealed by single-molecule FRET. *Proc. Natl. Acad. Sci. USA* **107**, 715–720 (2010).

ONLINE METHODS

DNA design and labeling. Acceptor-labeled 55-bp bottom strands of DNA and amino-C6-dT-modified biotinylated complementary top strands were purchased from IBA. DNA sequences and modifications are listed in **Supplementary Table 1**. Amino-modified strands were labeled with Cy3B *N*-hydroxy-succinimidyl ester³² and purified using denaturing PAGE. Complementary strands of DNA were annealed to form dsDNA by mixing equimolar amounts in annealing buffer (Tris-HCl pH 8.0, 500 mM NaCl and 1 mM EDTA) and heating to 95 °C followed by slow cooling to 4 °C.

Sample preparation. Biotinylated dsDNA was immobilized on neutravidin-coated glass coverslips, as described³³. Silicone gaskets (Grace Bio-Labs) and a second coverslip were used to seal the imaging chambers from oxygen. Two different imaging buffers were used in switching experiments¹⁴: buffer i, PBS (pH 7.4) and 50 mM β -mercaptoethylamine (MEA) for Cy5-Cy3B-Cy5 and CAP-DNA experiments, and buffer ii, 10 mM Tris-HCl (pH 7.5), 10 mM NaCl and 14.3 mM β -mercaptoethanol (BME) for ATTO655-Cy3B-ATTO655 and Holliday junction experiments (the latter with additional 200 mM MgCl₂). Photoswitching and photobleaching characteristics were optimized by incubating the imaging buffer at 37 °C for 6 h³⁴. All imaging buffers contained an enzymatic oxygen scavenging system (10% (w/v) glucose, 1 mg ml⁻¹ glucose oxidase and 40 μ g ml⁻¹ catalase). For Cy5-Cy3B-Cy5 control experiments under non-switching conditions, the imaging buffer (i) contained 0.5 mg ml⁻¹ TROLOX (6-hydroxy-2,5,7,8-tetramethylchroman-2-carboxylic acid) instead of MEA²².

ALEX microscopy. Imaging was performed on a custom-built total internal reflection fluorescence (TIRF) microscope using ALEX^{21,33} between a red laser (635 nm, directly modulated diode laser (Cube model; Coherent)) and a green laser (532 nm, continuous-wave solid state laser (Samba model; Cobolt) modulated using an acousto-optical modulator (AA Optics)). The alternation period was 200 ms in all experiments. The green and red laser beams were coupled into the same single-mode optical fiber. At the fiber output, the laser beams were collimated, directed into an inverted microscope (IX71, Olympus) and focused (100 \times oil-immersion objective, numerical aperture (NA) 1.4, Olympus) onto the sample under an angle allowing for total internal reflection. The fluorescence emission was collected by the same objective, separated from excitation light by a dichroic mirror (545 nm/650 nm, Semrock) and additional filters (545 nm LP, Chroma; and 633/25 nm notch filter, Semrock). To allow for dual-color detection, the emission light was split into red and green channels (630 nm DRLP; Omega) and projected onto two separate regions of an electron-multiplying charge-coupled device (EMCCD) camera (iXon Andor). Laser powers used were 2 mW (635 nm) and 1 mW (532 nm) for Cy5-Cy3B-Cy5, 1 mW (635 nm and 532 nm) for ATTO655-Cy3B-ATTO655 and 0.5 mW (635 nm and 532 nm) for CAP-DNA and Holliday junctions (intensities measured before the beams entered the TIRF objective).

Data analysis. To extract single-molecule intensity trajectories, TIRF movies were analyzed with custom written software in Matlab (Mathworks) by applying methods adapted from astronomy^{25,35}; the software will be available to the community shortly. First, the red and green emission channels were aligned based

on calibration movies of immobilized fluorescence beads. The emission of single immobilized labeled DNA molecules in the red and green channel was automatically detected and linked using a peak-finding algorithm³⁶. Peaks that did not meet ellipticity or nearest-neighbor criteria were excluded from further analysis ($\epsilon < 0.25$, $NN > 8$ pixels), thereby minimizing artifacts resulting from molecules with overlapping point spread functions. The emission intensity of each molecule was estimated by fitting a two-dimensional Gaussian to its point spread function. This yields F_{DD} (donor emission upon donor excitation), F_{DA} (acceptor emission upon donor excitation) and F_{AA} (acceptor emission upon acceptor excitation). These intensities were divided by the EMCCD gain factor of 16 to obtain actual photon counts. Apparent FRET efficiency, E^* , and stoichiometry, S , were calculated using F_{DD} , F_{DA} and F_{AA} by:

$$E^* = \frac{F_{DA}}{F_{DD} + F_{DA}} \quad (1)$$

$$S = \frac{F_{DD} + F_{DA}}{F_{DD} + F_{DA} + F_{AA}} \quad (2)$$

Note that variation in the relative excitation intensity at 635 nm and 532 nm causes a shift in S . Populations in the E^* - S histogram were identified using k -means clustering. The algorithm partitions the points on the two-dimensional histogram into clusters by minimizing the sum of distances of points to the centroid of their cluster. The standard deviations ($\sigma(E^*)$ and $\sigma(S)$) of individual clusters were obtained from a Gaussian fit of the one-dimensional projection on the E^* or S axis.

Combined E^* - S histograms display the combined data of multiple movies under identical conditions. From the total 290 molecules in the case of the Cy5-Cy3B-Cy5 data, 143 molecules where all fluorophores bleached within the first 10 s were excluded by applying a threshold on the total red and green emission intensity. No such filter was used for CAP-DNA and Holliday junction data. Only data with an active donor were included by thresholding $F_{DD} > 40$ counts per 100 ms. The donor-only state is omitted by thresholding $S < 0.8$ for clarity.

Accurate FRET analysis. Correction of apparent FRET efficiencies (E^* values) to obtain accurate FRET efficiencies (E values) was performed as described previously¹⁹, except that all correction factors can be obtained from an individual molecule. Corrections account for: (i) leakage of the donor emission into the acceptor-emission channel; (ii) direct excitation of the acceptor by the green laser; and (iii) unequal quantum yield and detection efficiency of the donor and acceptor ($\gamma \neq 1$). The leakage factor Lk was calculated from the mean E^* value of the donor-only state:

$$Lk = \frac{E_{0-D0}^*}{1 - E_{0-D0}^*} \quad (3)$$

The direct-acceptor-excitation factor Dir was calculated from the stoichiometry of an acceptor-only state by:

$$Dir = \frac{S_{A-00}}{1 - S_{A-00}} \quad (4)$$

Subtraction of donor-leakage and acceptor-direct-excitation counts from the F_{DA} signal and addition of leakage counts to F_{DD} yielded the FRET proximity ratio, E_{PR} , which was expressed in terms of mean E^* and S for each cluster:

$$E_{PR} = \frac{1 - \text{Dir} \times \frac{1-S}{S} - \text{Lk} \times \frac{1-E^*}{E^*}}{\frac{1-E^*}{E^*} + 1 - \text{Dir} \times \frac{1-S}{S}} \quad (5)$$

The linear dependence between $1/S$ and E_{PR} allows the estimation of γ from two distinct clusters by a linear fit. Finally, accurate FRET is determined from:

$$E = \frac{E_{PR}}{\gamma - (\gamma - 1) \times E_{PR}} \quad (6)$$

Error analysis was performed by calculating the error propagation of the s.d. of the clusters in the E^* - S histogram to obtain the s.e.m. for the accurate FRET values.

Theoretical FRET calculations. Theoretical FRET values for the two configurations A-D0 and 0-DA of Cy5-Cy3B-Cy5 molecules were quantified based on a cylindrical model of helical B-DNA^{19,24,37,38} using:

$$E_{th} = \frac{R_0^6}{R_0^6 + R^6} \quad (7)$$

$$R = \sqrt{(\Delta \times n + L)^2 + d^2 + a^2 - 2da \times \cos(\Theta \times n + \Phi)} \quad (8)$$

R_0 is the Förster radius, R is the donor-acceptor distance, Δ is the helical rise per bp, n is the bp separation between the donor and the acceptor, Θ is the rotation angle per bp, L is an additional distance along the helical axis, d and a are the radial extensions of the donor and the acceptor because of the finite linker lengths, and Φ is a constant angle accounting for the phase shift between the opposite DNA strands.

The Förster radius of $R_0 = 67 \text{ \AA}$ was calculated using the measured overlap integral of the emission spectrum of Cy3B and the absorption spectrum of Cy5 (each attached to singly labeled dsDNA identical to the one used in the switchable FRET experiments), the quantum yield of Cy3B (ref. 39) $\Phi_D = 0.67$, and the extinction coefficient of Cy5 (ref. 40) $\epsilon_A = 250,000 \text{ cm}^{-1} \text{ M}^{-1}$ at the absorption maximum (647 nm). We assume orientational averaging ($\kappa^2 = 2/3$), supported by the presence of significant local rotational freedom as indicated by the steady-state anisotropies of 0.24 for Cy3B, 0.22 for the internally labeled Cy5, and 0.19 for the end-labeled Cy5. Given the measured anisotropies, we estimated upper and lower bounds on the Förster radius as 53 Å and 85 Å, respectively⁴¹. The fixed parameters in Eq. 8 are $n = [10, 19]$, $\Theta = 36^\circ$ and $\Delta = 3.4 \text{ \AA}$. The experimental data can be well explained using the following structural parameters: $\Phi = 228^\circ$; $L = 4 \text{ \AA}$ for the end-labeled Cy5 and $L = 0 \text{ \AA}$ for the internally labeled Cy5; $d = 18 \text{ \AA}$ and $a = 18 \text{ \AA}$ for Cy3B and the internally labeled Cy5, and $a = 5 \text{ \AA}$ for the end-labeled Cy5, which adopts an effective position which is close to the helical axis. These parameters fit

well to the experimental data for A-D0 and 0-DA and they are in agreement with similar DNA models based on FRET^{19,24,37,38}. In the case that one donor transfers energy to both acceptors (A-DA), the total FRET efficiency is determined from the individual single-pair FRET efficiencies by

$$E_{th} = \frac{w_{A-D0} + w_{0-DA}}{1 + w_{A-D0} + w_{0-DA}} \quad (9)$$

with $w_i = E_i / (1 - E_i)$.

Monte-Carlo simulation. The Monte Carlo simulation of switchable FRET is based on a stochastic simulation of FRET at the ensemble level⁴². Here, we simulated stochastic excitation and FRET of a single donor (Cy3B) and an arbitrary number of photoswitchable acceptors (Cy5) at the single-molecule level. A schematic of the model for two acceptors is shown (Supplementary Fig. 5). Simulation parameters for data in Supplementary Figures 3, 4 and 8 are listed in Supplementary Table 4. ALEX time traces were modeled by alternating periods of green excitation and red excitation. Green excitation causes either donor emission, or FRET to one of the acceptors, or photoactivation of an acceptor. Red excitation leads to acceptor emission or deactivation of an acceptor. The time a fluorophore spends in the excited state is a random number calculated with Gillespie's algorithm (mean lifetimes $\tau_{Cy5} = 1 \text{ ns}$, $\tau_{Cy3B} = 2.8 \text{ ns}$ ^{39,40}). The single-pair FRET efficiencies between the donor and each of the individual acceptors were specified as an input for the simulation. Only acceptors in the active state can serve as energy acceptors. For simulation of molecular dynamics, each conformational state was characterized by a set of FRET efficiencies (of the different acceptors) and transitions between the states followed single-exponential kinetics.

In addition to inherent photon shot noise owing to the stochastic nature of the simulation, Poisson-distributed background counts were added to the emission streams. We also modeled the multiplicative noise of the stochastic gain register of an EMCCD camera⁴³. Subsequently, the mean amplified background was subtracted from the amplified signal and the signal is divided by the gain factor ($G = 16$ for our setup). The signal-to-noise ratio (SNR) of the simulated signals was modeled according to theory⁴⁴:

$$\text{SNR} = \frac{F}{\sigma_F} = \frac{F}{f_G \times \sqrt{G \times \left(F + \frac{4\pi s^2}{l^2} \times \sigma_B^2 \right)}} \quad (10)$$

Here F is the mean amplified signal, $f_G = \sqrt{2}$ is the noise factor of the EMCCD gain⁴³, s is the s.d. of the PSF (230 nm for Cy5 and 155 nm for Cy3B), $l = 110.6 \text{ nm}$ is the pixel length and $\sigma_B^2 = B$ is the mean amplified background per pixel and frame assuming a Poisson distribution (measured in a region without fluorescent spots).

To account for detection biases (γ), a fraction of the acceptor emission is stochastically discarded. Leakage of donor emission into the acceptor detection channel (Lk) is simulated by stochastically counting a fraction of the donor emission as acceptor emission. Our data showed that acceptor-direct-excitation was minor and hence not included in the simulation. E^* and S were calculated from F_{DD} , F_{DA} and F_{AA} as with experimental data. Note that the effect of leakage and $\gamma < 1$ causes a shift in E^* compared to the input values of E .

CAP-DNA experiments. Production, expression and purification of CAP(Cys17,Ser178) protein (where the amino acids in the parentheses are residues that had substituted the amino acids present in the wild-type protein sequence) has been described previously^{28,45}. Briefly, plasmid pAKCRP-His6-(Cys17,Ser178) was generated from pAKCRP-His6 using Quick Change II Site-directed Mutagenesis Kit (Stratagene). The sequence of the plasmid was confirmed by DNA sequencing. CAP(Cys17,Ser178) was labeled with tenfold molar excess of Alexa Fluor 647 maleimide in 40 mM HEPES-NaOH (pH 7), 200 mM KCl, 1 mM EDTA, 0.1 mM TCEP and 0.2 mM cAMP. The reaction sample was quenched with 10 mM DTT for 15 min and purified using a NAP5 gel filtration column (Amersham) equilibrated with storage buffer (20 mM HEPES-NaOH pH 7, 200 mM NaCl, 1 mM DTT, 1 mM MEA and 5% glycerol). The DNA-binding activity of labeled CAP(Cys17,Ser178) was evaluated using a shift assay described previously³².

A 39-bp dsDNA containing the CAP recognition sequence (ICAP DNA) was prepared similar to the other DNA constructs. Sequence and modifications are given in **Supplementary Table 1**. ICAP DNA was incubated with tenfold molar excess of CAP on neutravidin-coated coverslips. Switchable FRET experiments were performed in switching buffer i containing 0.2 mM cAMP.

Holliday junction experiments. The Holliday junction construct of four separate DNA strands (X, B, R and H strands; prepared similar to the other DNA constructs) was based on previous designs^{8,46}. DNA sequences and modifications are given in **Supplementary Table 1**. Control experiments using Holliday junctions labeled with Cy3B and e-Cy5 only were performed with unlabeled B-strand. Hybrids were formed using 1:0.8 molar ratios of strands X, B, R with H in 10 mM Tris-HCl (pH 8.0) with 100 mM NaCl and

heating to 95 °C followed by slow cooling to 4 °C. Experiments were performed in switching buffer ii containing 200 mM MgCl₂.

32. Heilemann, M., Hwang, L.C., Lymperopoulos, K. & Kapanidis, A.N. Single-molecule FRET analysis of protein-DNA complexes. *Methods Mol. Biol.* **543**, 503–521 (2009).
33. Kapanidis, A.N. *et al.* Alternating-laser excitation of single molecules. in *Single Molecule Techniques: A Laboratory Manual* 1st edn. (eds. Selvin, P. & Ha, T.) 85–119 (Cold Spring Harbor Laboratory Press, 2008).
34. Cordes, T., Vogelsang, J. & Tinnefeld, P. On the mechanism of Trolox as antiblinking and antibleaching reagent. *J. Am. Chem. Soc.* **131**, 5018–5019 (2009).
35. Irwin, M. Detectors and data analysis techniques for widefield optical imaging. in *Instrumentation for Large Telescopes: VIIth Canary Islands Winter School of Astrophysics* 35–74 (1997) (Cambridge University Press, New York, 1997).
36. Crocker, J.C. & Grier, D.G. Methods of digital video microscopy for colloidal studies. *J. Colloid Interface Sci.* **179**, 298–310 (1996).
37. Deniz, A.A. *et al.* Single-pair fluorescence resonance energy transfer on freely diffusing molecules: Observation of Förster distance dependence and subpopulations. *Proc. Natl. Acad. Sci. USA* **96**, 3670–3675 (1999).
38. Norman, D.G., Grainger, R.J., Uhrin, D. & Lilley, D.M.J. Location of cyanine-3 on double-stranded DNA: importance for fluorescence resonance energy transfer studies. *Biochemistry* **39**, 6317–6324 (2000).
39. Cooper, M. *et al.* Cy3B: Improving the performance of cyanine dyes. *J. Fluoresc.* **14**, 145–150 (2004).
40. Gell, C., Brockwell, D. & Smith, A. *Handbook of Single Molecule Fluorescence Spectroscopy* (Oxford University Press, 2006).
41. Dale, R.E., Eisinger, J. & Blumberg, W.E. The orientational freedom of molecular probes. *Biophys. J.* **26**, 161–193 (1979).
42. Berney, C. & Danuser, G. FRET or no FRET: A quantitative comparison. *Biophys. J.* **84**, 3992–4010 (2003).
43. Daigle, O., Carignan, C. & Blais-Ouellette, S. Faint flux performance of an EMCCD. *Proc. SPIE.* **6276**, 62761–62767 (2006).
44. Thompson, R.E., Larson, D.R. & Webb, W.W. Precise nanometer localization analysis for individual fluorescent probes. *Biophys. J.* **82**, 2775–2783 (2002).
45. Kapanidis, A.N., Ebright, Y.W. & Ebright, R.H. Site-specific incorporation of fluorescent probes into protein: Hexahistidine-tag-mediated fluorescent labeling using (Ni²⁺:Nitrilotriacetic acid)-fluorochrome conjugates. *J. Am. Chem. Soc.* **123**, 12123–12125 (2001).
46. McKinney, S.A., Déclais, A.-C., Lilley, D.M. & Ha, T. Structural dynamics of individual Holliday junctions. *Nat. Struct. Biol.* **10**, 93–97 (2003).